PHYSICAL REVIEW B **89**, 035417 (2014)

Absence of hyperfine effects in ^{13}C-graphene spin-valve devices

M. Wojtaszek,[1,*] I. J. Vera-Marun,[1] E. Whiteway,[2] M. Hilke,[2] and B. J. van Wees[1]

[1]*Physics of Nanodevices, Zernike Institute for Advanced Materials, University of Groningen, Groningen, The Netherlands*

[2]*Department of Physics, McGill University, Montreal, Quebec, Canada H3A 0G4*

(Received 20 November 2013; published 14 January 2014)

The carbon isotope ^{13}C, in contrast to ^{12}C, possesses a nuclear magnetic moment and can induce electron spin dephasing in graphene. This effect is usually neglected due to the low abundance of ^{13}C in natural carbon allotropes (∼1%). Chemical vapor deposition (CVD) allows for artificial synthesis of graphene solely from a ^{13}C precursor, potentially amplifying the influence of the nuclear magnetic moments. In this work we study the effect of hyperfine interactions in pure ^{13}C-graphene on its spin transport properties. Using Hanle precession measurements we determine the spin relaxation time and observe a weak increase of τ_s with doping and a weak change of τ_s with temperature, as in natural graphene. For comparison we study spin transport in pure ^{12}C-graphene, also synthesized by CVD, and observe similar spin relaxation properties. As the signatures of hyperfine effects can be better resolved in oblique spin-valve and Hanle configurations, we use finite-element modeling to emulate oblique signals in the presence of a hyperfine magnetic field for typical graphene properties. Unlike in the case of GaAs, hyperfine interactions with ^{13}C nuclei influence electron spin transport only very weakly, even for a fully polarized nuclear system. Also, in the measurements of the oblique spin-valve and Hanle effects no hyperfine features could be resolved. This work experimentally confirms the weak character of hyperfine interactions and the negligible role of ^{13}C atoms in the spin dephasing processes in graphene.

DOI: 10.1103/PhysRevB.89.035417 PACS number(s): 72.25.−b, 85.75.−d, 31.30.Gs

I. INTRODUCTION

Spin transport in graphene has attracted a lot of research attention due to predictions of high spin relaxation times τ_s and large spin relaxation lengths λ_s [1]. The experimentally determined values of τ_s (Refs. [2–4]) center around values of 100 ps–1 ns, three orders of magnitude lower than expected. This discrepancy between theory and experiment motivates the need to identify the mechanisms for spin dephasing [5,6].

A well-known source of dephasing is the presence of random magnetic moments (for example from localized states [7,8]). The ^{13}C isotope with nuclear spin $I_N = \frac{1}{2}$ also possesses a magnetic moment but this is usually neglected due to the low abundance of ^{13}C in natural carbon allotropes (∼1%) and a weak hyperfine coupling of $\lesssim$0.6 μeV, about 100 times smaller than for GaAs [9,10]. Although there are many theoretical evaluations of the size of hyperfine interactions [9,11,12] and their role in spin transport, they lack experimental verification in graphene.

In this work we demonstrate spin transport in pure ^{13}C-isotope graphene and compare it with spin transport in pure ^{12}C-isotope graphene using the nonlocal spin-valve geometry. We use Hanle precession measurements to characterize the spin properties at room temperature and at 4.2 K for different carrier densities. We also amplify the hyperfine effects by increasing the spin polarization in graphene, to induce dynamical nuclear polarization (DNP). The depolarizing effect of nuclei is best observed under an oblique external magnetic field, which makes the orientation of nuclear spin noncollinear to the electron spin, causing extra spin precession. To quantify this effect on the spin signals we model the nonlocal spin-valve and Hanle precession effects at oblique angles for various degrees of graphene polarization. The estimated hyperfine features in spin transport are below the experimentally achievable resolution, which we confirm later experimentally. These measurements are reproduced in several graphene regions as well as in independently fabricated samples. By exploring the extreme conditions of pure ^{13}C composition and high graphene polarization, we experimentally verify the weak character of hyperfine interactions in graphene and the negligible role of ^{13}C atoms in spin dephasing in graphene.

II. SAMPLE FABRICATION

The advent of synthetic methods to grow graphene [13–15] allows for chemical growth of graphene with an arbitrary composition of carbon isotopes. A pure ^{13}C-graphene monolayer is synthesized on commercial Cu foil using chemical vapor deposition (CVD) from 99.9% pure ^{13}C-methane (CLM-3590-1, from Cambridge Isotopes Laboratories, Inc.) as described in Ref. [16]. Next, to transfer the graphene to an insulating substrate, we attach the graphene on Cu foil to a polydimethylsiloxane stamp (PDMS) and dip it into $FeCl_3$ aqueous solution (1 g ml^{-1}) to etch away the copper. After the removal of Cu and subsequent dipping in deionized water to clean off the etching residues, we transfer the graphene onto a 500-nm-thick layer of SiO_2 with a highly doped Si substrate below to serve as a back gate.

A homogeneous, single-layer graphene area is selected based on optical contrast and Raman spectroscopy [17], using a 532 nm laser. The Raman spectrum of pure ^{13}C-graphene is shown in Fig. 1(a), where for comparison we also show the spectrum of pure ^{12}C-graphene. The latter is also a good representative of the spectrum of natural graphene, which has only ∼1% of ^{13}C abundance. When compared to ^{12}C-graphene, the vibrational Raman modes in ^{13}C-graphene display a downward shift [16]; here from ∼1585 to 1525 cm^{-1} for the G band and from ∼2680 to 2580 cm^{-1} for the 2D band.

*m.wojtaszek@rug.nl

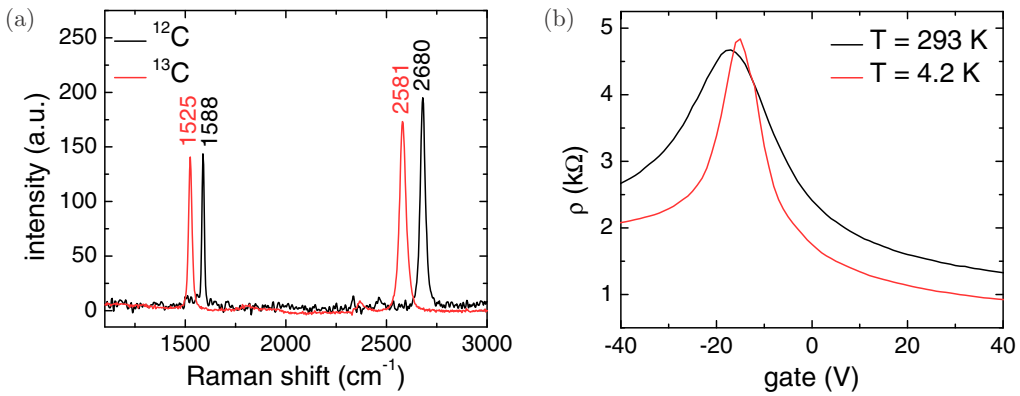

FIG. 1. (Color online) (a) Raman spectrum of CVD graphene on SiO_2 of pure ^{12}C (black) and pure ^{13}C (red) isotopic content. The ratios of the Raman shift ν for graphene G and $2D$ bands reflect the difference in the mass of these isotopes: $\nu_{^{12}C}/\nu_{^{13}C} = \sqrt{13/12}$. (b) The typical curve of ^{13}C-graphene sheet resistivity as a function of gate voltage at room temperature (black) and at $T = 4.2$ K (red).

This shift arises from the difference in the atomic masses of the carbon isotopes and is consistent with the classical model of a harmonic oscillator, where its vibrational modes are inversely proportional to the square root of its masses. Raman spectroscopy also confirms the good quality of the selected graphene area, by the absence of a D band in the spectrum [18].

After selecting a graphene region we define a rectangular strip of graphene using electron-beam lithography and O_2 plasma etching. Then we define contacts using an e beam in poly(methylmethacrylate) (PMMA) resist. First we evaporate 0.8 nm of Al and then naturally oxidize it, in order to turn it into a tunneling barrier. Next, we evaporate Co (30 nm) and 2 nm of Al on top as a capping layer to protect the cobalt from oxidation. The tunneling barrier of AlO_x is present only underneath the contacts. All samples are measured in high vacuum. Low-temperature measurements are performed in a flow cryostat with a rotatable magnet around the in-plane and out-of-plane axes of the sample.

III. CHARGE AND SPIN TRANSPORT IN ^{13}C-GRAPHENE

Initially we characterize the sheet resistance ρ of graphene as a function of the gate bias V_g in a four-terminal measurement. The induced carrier concentration n is calculated from $n = C_g(V_g - V_0)/e$, where V_0 is the voltage corresponding to the maximum of ρ (Dirac point), and C_g is the gate capacitance, $C_g = 70$ aF/μm^2 for 500 nm SiO_2. The measured samples display similar electronic quality to micromechanically cleaved graphene [2,19], with mobilities $\mu = (en\rho)^{-1}$ between 1000 and 3000 cm^2/Vs. As in exfoliated graphene on SiO_2 the maximum of $\rho(V_g)$ does not vary strongly with temperature and only the Dirac peak displays a narrowing of its width due to the reduced thermal broadening; see Fig 1(b).

Next we perform spin transport measurements in a nonlocal spin-valve geometry. In such a measurement we inject a spin-polarized current through a ferromagnetic contact, the injector, and probe it with another ferromagnetic contact, the detector. The injection and detection circuits are separated [see Fig. 2(a)], which reduces the magnetoresistive background and electrical noise.

A nonlocal spin resistance, defined as $R_{nl} = V_{nl}/I$, displays a switching "spin-valve" behavior when an in-plane magnetic field is swept, correlated with the switching of the relative magnetization of the injecting and detecting contacts from parallel ($\uparrow\uparrow$) to antiparallel ($\downarrow\uparrow$) alignment. By setting the magnetic field perpendicular to the graphene plane we can study the spin precession (Hanle effect) [2,3,19]. Typical measurements of the spin-valve and Hanle precession signals are presented in Fig. 2(b) for room and for liquid-helium temperature. At low temperatures the amplitude of the signal increases, but its features remain the same. To remove the spin-independent background we record Hanle curves for the $\uparrow\uparrow$ and $\downarrow\uparrow$ cases, where the pure spin signal is $R_{nl} = (R_{nl}^{\uparrow\uparrow} - R_{nl}^{\downarrow\uparrow})/2$, and is further used for fitting the spin coefficients.

The Hanle effect can be described by the one-dimensional Bloch equation for the spin chemical potential $\boldsymbol{\mu}_s$:

$$D_s \nabla^2 \boldsymbol{\mu}_s - \frac{\boldsymbol{\mu}_s}{\tau_s} + \frac{g\mu_B}{\hbar}\mathbf{B} \times \boldsymbol{\mu}_s = \mathbf{0}, \tag{1}$$

which includes spin diffusion, the term with D_s, spin relaxation, the term with τ_s, and spin precession, the term with magnetic field $\mathbf{B}$ where $g = 2$ is the gyromagnetic factor of a free electron and μ_B is the electron Bohr magneton. By fitting the Hanle curve to the solution of Eq. (1) we can independently determine the spin diffusion length D_s and spin relaxation time τ_s. For a more accurate extraction of spin coefficients we always make sure that the distance between the injector and detector L is larger than the spin relaxation length $\lambda_s = \sqrt{\tau_s D_s}$, as motivated in Ref. [20].

A full characterization of the spin properties at room and liquid-helium temperatures as a function of carrier concentration n is given in the Supplemental Material [21]. Typically the values for τ_s in ^{13}C-graphene range from 60 to 100 ps, depending on the sample doping. The τ_s achieved are roughly twice smaller than previously reported for CVD graphene [22] and exfoliated graphene [2,19], although the electron mobility in our samples is comparable. A lower τ_s can originate from structural defects and rippling of the graphene sheet [1,22,23], which are inherent to the growth conditions, the quality of the catalytic substrate (Cu foil), and the transfer methods, as well as from eventual contamination with the $FeCl_3$ etchant. The lower values of τ_s are also found in the control sample—a CVD-grown graphene from pure ^{12}C precursor (see the next section), and therefore cannot be attributed to the dephasing from hyperfine fields from the ^{13}C nuclei.

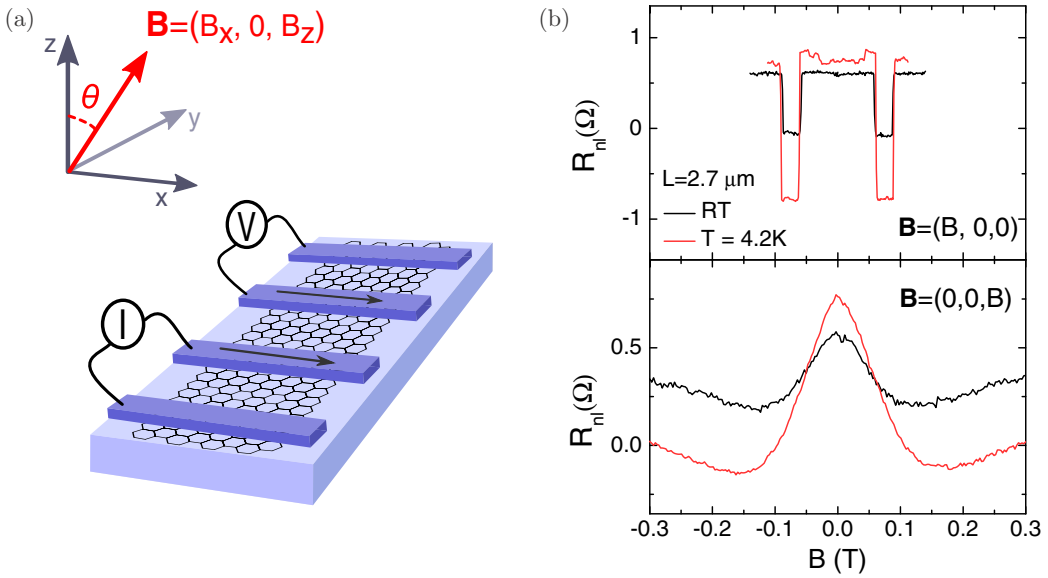

FIG. 2. (Color online) (a) Nonlocal detection scheme in a graphene spin-valve device. The arrows on the inner contacts mark their magnetization (here parallel). We measure signals for three different configurations of external field: in-plane $\mathbf{B} = (B,0,0)$ for the spin-valve effect, normal to the plane $\mathbf{B} = (0,0,B)$ for the regular Hanle effect, and at an angle θ, $\mathbf{B} = (B\sin\theta, 0, B\cos\theta)$ for the oblique Hanle effect. (b) Spin-valve and Hanle measurements in ^{13}C-graphene at room temperature (black) and at $T = 4.2$ K (red). The distance between ferromagnetic injector and detector is $L = 2.7$ μm and the contact magnetization is parallel.

IV. SPIN TRANSPORT PROPERTIES IN ^{13}C VERSUS ^{12}C GRAPHENE

At $B \leq 0.5$ T and $T \simeq 300$ K the nuclei are randomly oriented so that spin dephasing can happen due to these fluctuating, weak nuclear moments. The effect of randomly fluctuating nuclear moments can be evaluated by comparing the spin properties between pure ^{13}C- and pure ^{12}C-graphene in room-temperature spin transport. A pure ^{12}C-graphene monolayer is synthesized on Cu by CVD from 99.99% pure ^{12}C-methane and then we follow the same device fabrication steps as for the ^{13}C samples. The magnetic moment of the ^{13}C nuclei [24] is $\mu_{^{13}\mathrm{C}} = 0.7\mu_n$, where $\mu_n = e\hbar/M$ is the nuclear magneton. As μ_n is about 1800 times smaller than μ_B, due to the much larger proton mass M, we have $\mu_{^{13}\mathrm{C}} \simeq \mu_B/2600$.

A comparison of room-temperature spin properties determined from Hanle fitting at different carrier concentration n for these two isotopically pure graphenes is presented in Fig. 3. For ^{13}C we analyze data for injector-detector spacing $L = 2.7$ μm and for ^{12}C $L = 4$ μm, both longer than λ_s. The large p doping in the ^{12}C device enables us to record the spin properties only in the hole regime. The values for D_s, τ_s, and λ_s for both ^{13}C and ^{12}C are very similar, proving the negligible effect of random nuclei on electron spin transport. Here, we experimentally verify that the random, unpolarized nuclei do not contribute to the spin dephasing. In the next sections we will analyze the experimental situation when the nuclear polarization could be built up coherently.

V. TRACKING COHERENT NUCLEAR FIELDS BY AN OBLIQUE HANLE EFFECT

Although the ^{13}C nuclei carry a smaller magnetic moment than the electrons, they outnumber them. In graphene the density of nuclei is $N = 3.32 \times 10^{15}$ cm^{-2}, so for pure ^{13}C-graphene the product $N\mu_I$ is comparable to $n\mu_B$ for the density of conducting electrons, $n = 1.3 \times 10^{12}$ cm^{-2}, and greater for n closer to the Dirac point. This means that once these nuclei are coherently polarized, they can produce

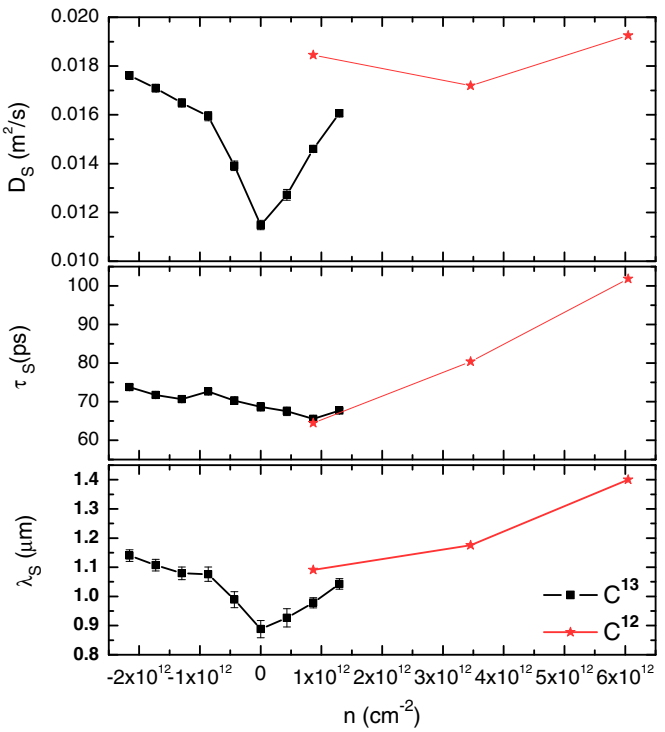

FIG. 3. (Color online) Comparison of spin properties at different carrier concentrations n between pure ^{13}C- and pure ^{12}C-graphene at room temperature. The coefficients are obtained from fitting Hanle measurements to the solution of Eq. (1). For ^{13}C we analyze data for injector-detector spacing $L = 2.7$ μm and for ^{12}C $L = 4$ μm.

a sizable nuclear magnetic field $\mathbf{B}_n$ and be a source of spin dephasing. $\mathbf{B}_n$ adds vectorially to the external magnetic field $\mathbf{B}$ and can modify the line shape of the Hanle curve, for example by changing its width or the position of the maximum or inducing an asymmetry versus the external magnetic field [10,25,26].

First, we provide an estimate for nuclear effects and model the unique features of the electrical spin signal due to the presence of $\mathbf{B}_n$. We can neglect the Zeeman splitting as a source of nuclear polarization ($\mathbf{B} \leq 0.5$ T, $T \simeq 4.2$ K, so $|E_Z| = \gamma_{^{13}\mathrm{C}}\hbar B < 25$ neV, where $\gamma_{^{13}\mathrm{C}} = 6.73 \times 10^7$ rad/Ts is the gyromagnetic ratio of the ^{13}C isotope). Hence the nuclear polarization can arise only from the "flip-flop" angular momentum exchange with polarized electrons (DNP) [10]. After such an angular momentum transfer the magnetic field produced by polarized nuclei (the Overhauser field) has the same orientation as the electronic spins so no hyperfine dephasing is induced. However, when one applies the external magnetic field at an oblique angle, the nuclear spin will immediately precess around the total magnetic field $\mathbf{B} + \mathbf{B}_e$, where $\mathbf{B}_e$ is the average magnetic field created by electrons (the Knight field). Following Paget *et al.* [10], we can express the nuclear field $\mathbf{B}_n$ as

$$\mathbf{B}_n = f b_n \frac{(\mathbf{B} + \mathbf{B}_e) \cdot \langle \mathbf{S} \rangle (\mathbf{B} + \mathbf{B}_e)}{(\mathbf{B} + \mathbf{B}_e)^2} \tag{2}$$

where $\mathbf{B}_e = b_e \langle \mathbf{S} \rangle$, $\langle \mathbf{S} \rangle$ is the average electron spin polarization ($|\langle \mathbf{S} \rangle| = \frac{1}{2}$ for a fully polarized system), b_n and b_e are describing the effective magnetic fields produced by the nuclear and electron spin, respectively, in the case of their complete polarization, and $f = T_1/(T_1 + T_{1e}) \lesssim 1$ is the leakage factor, which relates the spin relaxation due to hyperfine interactions between the nuclei and the fluctuating magnetic field of the electrons T_{1e} and other relaxation processes T_1 [25,27]. From formula (2) we see that $\mathbf{B}_n$ is proportional to the average electronic spin $|\langle \mathbf{S} \rangle| = \beta \times \frac{1}{2}$, where β is the electron polarization or the ratio between the number of polarized carriers and the total number of carriers, $\beta \simeq \frac{2\mu_s \nu(E_F)}{n(E_F)}$, where $\nu(E)$ is the density of states of graphene and n is the number of states at a given Fermi level E_F. In the limit of zero temperature, $E_F = \sqrt{\pi n}\hbar v_F$, where v_F is the Fermi velocity of graphene, and one gets $\nu(E_F)/n(E_F) = 1/E_F$. As $\mu_s = e\Delta V_{\mathrm{nl}}/P$ where $\Delta V_{\mathrm{nl}} = V_{\mathrm{nl}}^{\uparrow\uparrow} - V_{\mathrm{nl}}^{\downarrow\uparrow}$ and P is the polarization of the detector, we can directly relate the nonlocal signal to graphene polarization: $\beta = \frac{2e\Delta V_{nl}}{\sqrt{\pi n}\hbar v_F P}$.

With both internal and external noncollinear magnetic fields the Bloch equation [Eq. (1)] now requires a full vectorial treatment. The mutual, nonlinear dependence of $\mathbf{B}_n$ and $\boldsymbol{\mu}_s$ requires solving the Bloch equation self-consistently. For that we choose a finite-element method package (COMSOL) [28,29]. We define the problem as time independent; therefore we assume that the experimental time scale is longer than the time necessary for the nuclei to adapt to the external magnetic field ($\sim$100 μs from the typical linewidth of the NMR ^{13}C spectrum [30]). In Eq. (2) we can distinguish two regimes: (1) for small external fields, $b_e\langle \mathbf{S} \rangle > \mathbf{B}$, when $\mathbf{B}_n$ is almost aligned with $\langle \mathbf{S} \rangle$, and (2) for large external fields, $b_e\langle \mathbf{S} \rangle \ll \mathbf{B}$, when $\mathbf{B}_n$ is almost aligned with $\mathbf{B}$. For the first regime a dephasing feature of nuclear origin can be observed in spin-valve measurements as a dip around $B = 0$ if we add to the sweeping in-plane field a small out-of-plane component B_z. In the second field regime $\mathbf{B}_n$ can be identified using an oblique Hanle effect, where it leads to an asymmetry in precession curves and the appearance of additional satellite peaks. These features are best observed at large L because the Hanle line shape can be fully recorded within a smaller field range, avoiding the switching of the magnetization of the contact.

First we test our model for the case of doped GaAs, where the hyperfine effects are well understood [10,25,26], and the effective coefficients b_n and b_e are known. As the model emulates properly all the features related to $\mathbf{B}_n$ in GaAs [21], we can now apply it also to the case of ^{13}C-graphene. However, there are some important remarks. In GaAs all the constituent isotopes ^{69}Ga, ^{71}Ga, and ^{75}As have larger magnetic moments ($I_N = \frac{3}{2}$) and the hyperfine interactions are stronger (90 μeV) [10], mainly due to the nonzero amplitude of the s orbital of the electrons at the position of the nuclei (Fermi contact). In graphene, where the conducting electrons are of π type, this amplitude is zero [9], and only the much smaller anisotropic hyperfine term -0.3 μeV (along the direction of electronic polarization) remains. This corresponds to $b_n \simeq -5.2$ mT, which is about 1000 times smaller than for GaAs [25]. Additionally, for conducting electrons one can ignore the term b_e [10]. Therefore for graphene Eq. (2) simplifies to

$$\mathbf{B}_n = f b_n \frac{\mathbf{B} \cdot \langle \mathbf{S} \rangle \mathbf{B}}{\mathbf{B}^2}. \tag{3}$$

Another important difference between graphene and GaAs is the time for building up the dynamical polarization. In doped GaAs the spin relaxation time T_{1e} is faster for localized electrons on donors ($T_{1e} = 0.1$ s) than for delocalized conduction electrons ($T_{1e} = 10^4$ s)[27]. DNP happens on the same time scale as T_{1e} (because it is a reciprocal process to relaxation). As graphene primarily lacks localized states, we expect that one needs hours to build up DNP by solely conduction electrons.

Now we want to estimate the spin polarization at which the nuclear field would cause experimentally resolvable features. Typically in our CVD graphene $\lambda = 1$ μm, $D_s = 0.03$ m^2/s, $\tau_s = 100$ ps, and $P = 0.1$. For modeling $\mathbf{B}_n$ we use Eq. (3) with $b_n = -5.2$ mT and we ignore any leakage effects ($f = 1$), which is the best-case scenario. The electronic polarization β in graphene can be enhanced by injecting a large spin-polarized dc current I_{dc}. β also depends on the position of the Fermi level and therefore can be tuned by the gate voltage. Its value is largest at the Dirac point; however, it is limited by the residual carrier doping from impurities, inhomogeneities, and substrate ($n_{\mathrm{res}} \approx 10^{11}$ cm^{-2}), so in the simulation we take $E_F \simeq 50$ meV. We model the transport features in the oblique spin-valve and oblique Hanle magnetic field configurations as a function of I_{dc}; see Fig. 4. In Fig. 4(a) we see a dip even without nuclear field B_n (dashed line) due to a small constant out-of-plane field component B_z (the inverted Hanle effect) [31]. On top of that there is a modulation due to the hyperfine effects, but even for the largest $I_{\mathrm{dc}} = 100$ μA this modulation is very small ($<$15 mΩ) and cannot be resolved experimentally. An even smaller change due to the polarized nuclear field appears in the oblique Hanle effect [see Fig. 4(b)], where it leads to a minute shift of the peak position (without formation of any asymmetric

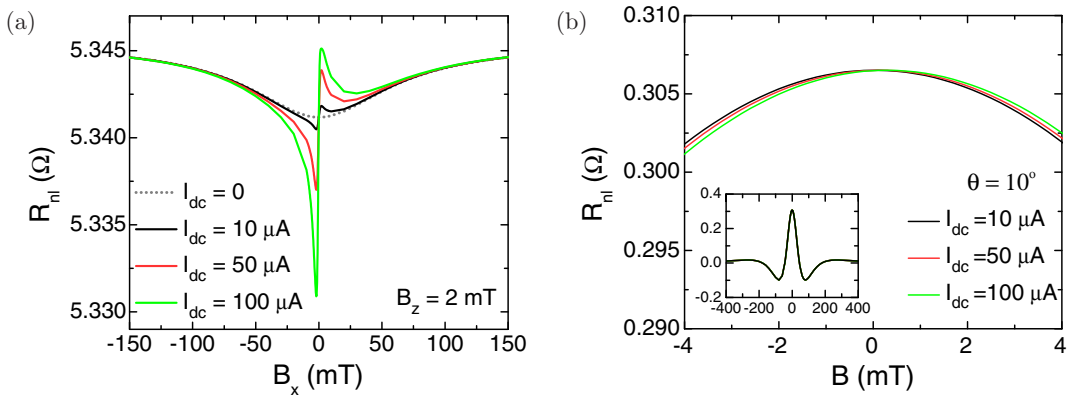

FIG. 4. (Color online) (a) Simulation of the nonlocal spin-valve signal at fixed $B_z = 2$ mT under the influence of a nuclear field $\mathbf{B}_n$ for different injection currents I_{dc} at $L = 1$ μm in $\uparrow\uparrow$ alignment. Values of $I_{dc} = 10,50,100$ μA correspond to the graphene polarization $\beta = 2\%,10\%,20\%$, respectively. The values of σ, D_s, and τ_s used in the model are determined experimentally for CVD graphene. (b) Simulation of the Hanle effect for magnetic field at the oblique angle $\theta = 10^\circ$ under the influence of nuclear field $\mathbf{B}_n$ for different polarization currents I_{dc} at $L = 5$ μm. The inset presents full Hanle curves for all I_{dc}, and the main figure zooms to the region where the curves for each I_{dc} do differ.

peaks in the line shape; see the inset). From the simulation we can see that the nuclear effects are very small and difficult to resolve experimentally due to a very small value of b_n.

To confirm experimentally the weak character of hyperfine effects we perform spin transport measurements at oblique magnetic fields and enhanced electron spin polarization. For that we send through the device a relatively large dc current (up to 50 μA) besides the small ac modulation (1 μA) used for lock-in detection. In Fig. 5(a) we show a nonlocal spin-valve signal under a field with small out-of-plane component $B_z \sim 1$ mT for varying I_{dc}. No dip around $B = 0$ could be observed for any strength of polarization current I_{dc} used. We should note that by sending a large dc current on the one hand we increase graphene polarization β but on the other hand we bias the tunneling injector and slightly decrease its spin injection efficiency (decrease of contact polarization). This can be recognized in the decrease of the spin-valve amplitude (ac signal) for increasing I_{dc}; see Fig. 5(a). The observed decrease is relatively small (up to 30% of the spin signal at $I_{dc} = 0$) which still maintains the increase of β with I_{dc}. For the largest I_{dc} the spin accumulation $\mu_s = eR_{nl}I_{dc}/P \simeq 3$ meV. This results in $\beta = 2.5\%$ at the injector ($L = 0$ μm) and $\beta = 0.6\%$ at the detector $L = 1.5$ μm.

As for conduction electrons the DNP is expected to build up very slowly ($T_{1e} \sim 10^4$ s), we also perform measurements of minor loops (narrower sweeps of the magnetic field, where only the detector contact switches its magnetization) at constant polarizing dc current $I_{dc} = 30$ μA. The measurement lasts 4 h and still no features around zero field, which could be attributed to the nuclear field, could be resolved [21].

Next we experimentally investigate the line shape of the Hanle effect under the magnetic field at oblique angle $\theta = 5^\circ$ for various I_{dc} in parallel configuration; see Fig. 5(b). Although in our CVD graphene λ_s was relatively short, $\lambda_s \cong 1$ μm, thanks to high polarization of the contacts ($P = 8\%$–10%) it was possible to observe a spin signal even at large distances (for $L \simeq 5$ μm). No asymmetry in the Hanle line shape could be unambiguously resolved. The measured Hanle curves show

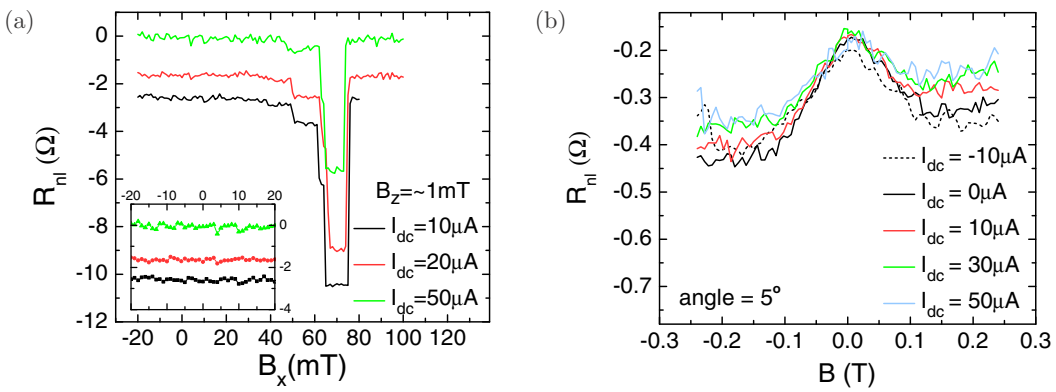

FIG. 5. (Color online) (a) Measurements of the nonlocal spin-valve signal with varying polarization currents I_{dc} at fixed $B_z = 1$ mT at $L = 1.5$ μm. The inset presents a zoom into region around $B_x = 0$. No dip around zero could be observed for any strength of polarization current I_{dc}. (b) Measurements of the Hanle effect for magnetic field at an oblique angle $\theta = 5^\circ$ upon varying polarization currents I_{dc} at $L = 4$ μm ($\uparrow\uparrow$). No asymmetry in the Hanle line shape could be clearly resolved. The linear background present for all I_{dc} comes from the Ohmic (not spin-dependent) contribution to the nonlocal signal.

only linear background from the Ohmic (not spin-dependent) contribution to the nonlocal signal. The scan size is limited by the magnetic anisotropy of the ferromagnetic contacts, which undergo switching at too high oblique **B**.

VI. DISCUSSION

The absence of any hyperfine-induced features in the line shape of the spin-valve resistance or Hanle curves confirms that it is not possible to create substantial nuclear polarization by conduction electrons and that the hyperfine coupling is too weak to be measurable. The DNP in graphene, even if hyperfine interactions had a comparable strength to GaAs, could not be efficiently induced due to the lack of localized electrons (and hence small correlation times between electron and nuclei). Enhancing the electron spin polarization to increase the probability of momentum transfer from electron to nuclei also has limitations. In graphene I_{dc} cannot be significantly enhanced due to the use of highly resistive tunnel contacts, which break down at large currents. In GaAs it is possible to achieve higher polarization [0.2%–6% (Ref. [25]) with $I_{dc} >$ 1 mA] because of the different nature of the Schottky contacts and lower resistance of the junction. Also, graphene's thermal properties limit the maximum I_{dc} (in the current annealing process one can go up to $I_{dc} \sim 1$ mA/μm before graphene breaks) [32]. The upper limit for I_{dc} tried here is 50 μA, which corresponds to a sizable voltage drop across the junction of $\sim$0.3 V and spin accumulation of $\sim$3 meV at the contact). These differences between GaAs and graphene explain the absence of any features associated with intrinsic nuclear magnetic fields in graphene, which are very pronounced in GaAs. The presented attempt to build up and detect DNP serves as an additional experimental confirmation of the negligible size of hyperfine interactions in graphene, alongside the observation of the same τ_s in pure ^{12}C- and ^{13}C-graphene.

We also attempted to induce a nuclear magnetic resonance, for which we measure the R_{nl} at oblique angle and $I_{dc} =$ 50 μA [21]. Also this attempt to modify (here reduce due to the rf field) the spin nuclear polarization showed no effect on the spin transport, which means that the nuclear fields in graphene are negligible and/or that the dc currents used here are unable to polarize the nuclei.

VII. CONCLUSIONS

In this work we experimentally verify the role of hyperfine interactions in spin transport in graphene. We observe that the spin relaxation time in graphene is not reduced by hyperfine interactions; even when we compare fully isotopic ^{13}C- against fully isotopic ^{12}C-graphene. Further, we perform a set of experiments in various configurations to amplify the hyperfine effects. In oblique spin-valve and Hanle measurements we tried to observe features of dynamically induced nuclear polarization, by creating a sizable electron polarization in graphene of $\sim$2.5%, but no distinctive features related to nuclei are observed. With the finite-element method we model the spin Bloch equation for graphene at oblique angles and we are able to estimate the lower limit for graphene polarization to result in any measurable fingerprints of the nuclear magnetic field. Even for the highest achievable spin polarization in graphene, the hyperfine features cannot be experimentally resolved. This is further confirmed by the measurements at oblique angle at high polarizing currents. This paper experimentally proves the negligible role of the intrinsic hyperfine interactions in graphene for spin relaxation, in agreement with theory. Yet the possibility of observing a spin signal over relatively large distances in CVD graphene confirms the choice of graphene as an efficient spin transport material for future applications.

ACKNOWLEDGMENTS

We would like to thank P. Crowell, G. Salis, G. Chad, and A. R. Onur for useful discussions. We would like to acknowledge M. H. D. Guimaraes, H. M. de Roosz, J. Holstein, and B. H. J. Wolfs for technical support. This work was financed by NanoNed, the Zernike Institute for Advanced Materials, and the Foundation for Fundamental Research on Matter (FOM).

[1] D. Huertas-Hernando, F. Guinea, and A. Brataas, Phys. Rev. B **74**, 155426 (2006).
[2] N. Tombros, C. Józsa, M. Popinciuc, H. T. Jonkman, and B. J. van Wees, Nature (London) **448**, 571 (2007).
[3] W. Han and R. K. Kawakami, Phys. Rev. Lett. **107**, 047207 (2011).
[4] M. H. D. Guimarães, A. Veligura, P. J. Zomer, T. Maassen, I. J. Vera-Marun, N. Tombros, and B. J. van Wees, Nano Lett. **12**, 3512 (2012).
[5] P. Zhang and M. W. Wu, New J. Phys. **14**, 033015 (2012).
[6] D. Kochan, M. Gmitra, and J. Fabian, arXiv:1306.0230.
[7] K. M. McCreary, A. G. Swartz, W. Han, J. Fabian, and R. K. Kawakami, Phys. Rev. Lett. **109**, 186604 (2012).
[8] B. Birkner, D. Pachniowski, A. Sandner, M. Ostler, T. Seyller, J. Fabian, M. Ciorga, D. Weiss, and J. Eroms, Phys. Rev. B **87**, 081405 (2013).
[9] J. Fischer, B. Trauzettel, and D. Loss, Phys. Rev. B **80**, 155401 (2009).
[10] D. Paget, G. Lampel, B. Sapoval, and V. I. Safarov, Phys. Rev. B **15**, 5780 (1977).
[11] O. V. Yazyev, Nano Lett. **8**, 1011 (2008).
[12] B. Dóra and F. Simon, Phys. Status Solidi B **247**, 2935 (2010).
[13] M. Lin, W. Guo, M. Wu, P. Wang, T. Liu, C. Pao, C. Chang, S. Lee, and S. Lin, Appl. Phys. Lett. **101**, 221911 (2012).
[14] X. Li, W. Cai, J. An, S. Kim, J. Nah, D. Yang, R. Piner, A. Velamakanni, I. Jung, E. Tutuc *et al.*, Science **324**, 1312 (2009).
[15] S. M. Wang, Y. H. Pei, X. Wang, H. Wang, Q. N. Meng, H. W. Tian, X. L. Zheng, W. T. Zheng, and Y. C. Liu, J. Phys. D **43**, 455402 (2010).
[16] S. Bernard, E. Whiteway, V. Yu, D. G. Austing, and M. Hilke, Phys. Rev. B **86**, 085409 (2012).
[17] A. C. Ferrari, J. C. Meyer, V. Scardaci, C. Casiraghi, M. Lazzeri, F. Mauri, S. Piscanec, D. Jiang, K. S. Novoselov, S. Roth *et al.*, Phys. Rev. Lett. **97**, 187401 (2006).

[18] M. A. Pimenta, G. Dresselhaus, M. S. Dresselhaus, L. G. Cançado, A. Jorio, and R. Saito, Phys. Chem. Chem. Phys. **9**, 1276 (2007).
[19] C. Józsa, T. Maassen, M. Popinciuc, P. J. Zomer, A. Veligura, H. T. Jonkman, and B. J. van Wees, Phys. Rev. B **80**, 241403 (2009).
[20] T. Maassen, I. J. Vera-Marun, M. H. D. Guimarães, and B. J. van Wees, Phys. Rev. B **86**, 235408 (2012).
[21] See Supplemental Material at http://link.aps.org/supplemental/10.1103/PhysRevB.89.035417 for a comparison of spin properties in ^{13}C-graphene at room and low temperature, for description of the COMSOL model of Hanle precession and simulations of the oblique Hanle curves in case of GaAs, for a set of minor loop scans, and for studies of spin transport under NMR conditions.
[22] A. Avsar, T. Yang, S. Bae, J. Balakrishnan, F. Volmer, M. Jaiswal, Z. Yi, S. R. Ali, G. Güntherodt, B. H. Hong *et al*., Nano Lett. **11**, 2363 (2011).
[23] P. Zhang, Y. Zhou, and M. W. Wu, J. Appl. Phys. **112**, 073709 (2012).
[24] R. K. Harris and B. E. Mann, *NMR and the Periodic Table* (Academic Press, London, 1978).
[25] M. K. Chan, Q. O. Hu, J. Zhang, T. Kondo, C. J. Palmstrøm, and P. A. Crowell, Phys. Rev. B **80**, 161206 (2009).
[26] G. Salis, A. Fuhrer, and S. F. Alvarado, Phys. Rev. B **80**, 115332 (2009).
[27] M. Dyakonov and V. Perel, in *Modern Problems in Condensed Matter Sciences*, edited by F. Meier and B. P. Zakharchenya, Optical Orientation Vol. 8 (Elsevier, Amsterdam, 1984), pp. 11–71.
[28] A. Slachter, F. L. Bakker, and B. J. van Wees, Phys. Rev. B **84**, 174408 (2011).
[29] T. Valet and A. Fert, Phys. Rev. B **48**, 7099 (1993).
[30] W. de Boer, M. Borghini, K. Morimoto, T. O. Niinikoski, and F. Udo, J. Low Temp. Phys. **15**, 249 (1974).
[31] S. P. Dash, S. Sharma, J. C. Le Breton, J. Peiro, H. Jaffrès, J.-M. George, A. Lemaître, and R. Jansen, Phys. Rev. B **84**, 054410 (2011).
[32] N. Tombros, A. Veligura, J. Junesch, M. H. D. Guimarães, I. J. Vera-Marun, H. T. Jonkman, and B. J. van Wees, Nat. Phys. **7**, 697 (2011).